Ultralow Thermal Conductivity of Fullerene Derivatives

Xiaojia Wang,[†,*] *Christopher D. Liman,*[‡] *Neil D. Treat,*[‡] *Michael L. Chabinyc,*[‡] *and David G. Cahill*[†,*]

[†]Department of Materials Science and Engineering, and Materials Research Laboratory, University of Illinois, Urbana, Illinois 61801, USA
[‡]Materials Department, and Materials Research Laboratory, University of California, Santa Barbara, Santa Barbara, CA 93106-5121, USA

ABSTRACT

Recently, Duda *et al*. reported that the fullerene derivative [6,6]-phenyl-C_{61}-butyric acid methyl ester (PCBM) has the lowest thermal conductivity Λ ever observed in a fully-dense solid, $\Lambda \approx 0.03$ W m^{-1} K^{-1}. We have investigated a variety of phases and microstructures of PCBM and the closely related compound [6,6]-phenyl-C_{61}-butyric acid n-butyl ester (PCBNB) and find that the thermal conductivities of PCBM and PCBNB films are mostly limited to the range $0.05<\Lambda<0.06$ W m^{-1} K^{-1} with a few samples having slightly higher Λ. The conductivities we observe are ≈70% larger than reported Duda *et al*. but are still "ultralow" in the sense that the thermal conductivity is a factor of ≈3 below the conductivity predicted by the minimum thermal conductivity model using an estimate of the thermally excited modes per molecule.

Key words: Organic semiconductor, Fullerene, Ultralow thermal conductivity, Time-domain thermoreflectance

1. INTRODUCTION

In electrically-insulating amorphous materials, heat conduction can be described by a random walk of vibrational energy on the time and length scales of atomic vibrations and interatomic spacing,[1] leading to the so called "lower limit" of thermal conductivity. A number of recent studies have reported conductivities significantly below this conventional lower limit. Chiritescu *et al*.[2] found that the cross-plane thermal conductivity of layered WSe_2 crystals can be as low as 0.05 $W\,m^{-1}\,K^{-1}$ at room temperature, a factor of 6 smaller than the theoretically predicted minimum thermal conductivity. We use the term “ultralow thermal conductivity” to describe conductivities significantly below the conventional lower limit. In Ref. [2], the authors speculated that the localization of lattice vibrations, induced by the random stacking of two-dimensional crystalline thin sheets, was the reason for the ultralow thermal conductivity of layered WSe_2 crystals. This speculation was later shown to be incorrect: the number of localized states in not significant.[3] Dames and co-workers have suggested anisotropy of elastic constants produces a strong phonon focusing effect that suppresses the average component of the phonon velocities that propagate in direction of the stacking.[4]

Recently, Duda *et al*. studied the thermal conductivity of thin films made from a fullerene derivative, [6,6]-phenyl-C_{61}-butyric acid methyl ester (PCBM), using time-domain thermoreflectance (TDTR). They reported a thermal conductivity of 0.030 ± 0.003 $W\,m^{-1}\,K^{-1}$ for PCBM at room temperature,[5] the lowest thermal conductivity ever reported for a fully dense solid. The molecular packing in solid films of fullerene derivatives is nearly isotropic and they lack the layering that is thought to be important in creating ultralow thermal conductivity in WSe_2,

The objective our study is to verify the exceptionally low thermal conductivities reported

by Duda *et al*. for fullerene derivatives and to explore how the microstructure of these materials might affect their thermal conductivities. In addition to PCBM, we also investigate [6,6]-phenyl-C_{61}-butyric acid n-butyl ester (PCBNB), which is chemically similar to PCBM. Both PCBM and PCBNB exhibit a variety of microstructures and phases depending on the method used to form the thin layer.[6-9] Thus, PCBM and PCBNB provide a useful platform for examining the influence of microstructure and phase on the appearance of ultralow thermal conductivity in this class of materials.

We use time-domain thermoreflectance (TDTR) to study the thermal conductivity of thin films of C_{60}, PCBM, and PCBNB. To improve the sensitivity to the thermal conductivity, we carry out TDTR at different modulation frequencies and study samples of different film thickness to independently determine thermal conductivity and heat capacity from the data. Our measurements show that the thermal conductivity of an evaporated film of C_{60} is close to that reported by Olson *et al*. for C_{60}/C_{70} compacts.[10] The thermal conductivities of the PCBM and PCBNB films are a factor of ≈2 smaller than C_{60} but also a factor of ≈2 higher than that reported for PCBM in Ref.[5].

2. EXPERIMENTAL DETAILS

2.1. General Sample Features

PCBM is initially highly disordered in spin-coated thin films from organic solvents and subsequently crystallizes upon thermal annealing.[6,7] PCBM exhibits a number of polymorphic crystalline structures and crystalline forms with trapped solvent.[11] PCBNB is chemically similar to PCBM, with only a change from the methyl to butyl ester (see Fig. 1), and also has multiple polymorphs including two forms that can be reversibly interconverted by thermal treatment.[9] The

domains sizes of these crystallites tend to have larger lateral dimensions than those in similarly prepared films of PCBM.[8,9]

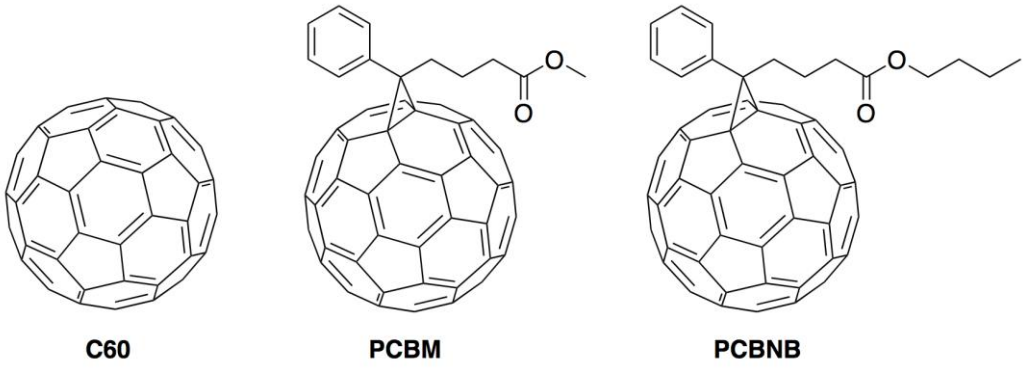

Figure 1. Chemical structures of C_{60}, PCBM, and PCBNB.

2.2. Sample Preparation and Characterization

We prepared thin-film samples using as-received C_{60} (99.5% purity, Nano-C, USA), PCBM (99.5% purity, Nano-C, USA), PCBNB (99% purity, Solenne, Netherlands), and PEDOT:PSS (Clevios P VP AI 4083 Heraeus) via spin coating or vapor deposition. Vapor deposition precludes solvent incorporation and forms highly disordered phases. C_{60} films were thermally evaporated onto silicon substrates. PCBNB samples were spun-cast on two substrates: silicon and PEDOT:PSS/silicon, and annealed at different temperatures to form various polymorphs. PCBNB Samples annealed at 80°C, 160°C, and 180°C are typically highly disordered, crystalline phase I (a superlattice structure of hexagonal lattices), and phase II (a simple hexagonal lattice), respectively.[8] PCBM samples were prepared by both solvent casting and thermal evaporation.

Prior to deposition, the silicon substrates were washed sequentially with acetone, 2 wt% soap:DI water solution, DI water, and isopropanol in an ultrasonic bath for 5 minutes. The clean

substrates were dried with a stream of N_2 and transferred into a N_2 glovebox. For solution processed PCBM thin films, PCBM was dissolved in chlorobenzene (99.8% anhydrous) at a concentration of 30 mg mL^{-1} and stirred at 90°C for 3 hours in a N_2 environment. PCBNB was dissolved in chlorobenzene at concentrations of 16 mg mL^{-1} and 20 mg mL^{-1} and stirred at 90°C for >3 hours in a N_2 environment. The solutions were cooled to room temperature and passed through a 0.45 μm PTFE filter onto the substrates.

The PCBM solutions were spin-coated on the clean substrates at a rate of 2000 rpm for 40 seconds. The 16 mg mL^{-1} solution of PCBNB was spin-coated on the substrates at rates of 700 or 1000 rpm for 60 seconds in the first step and 2000 rpm for 5 seconds in the second step, producing films with thicknesses ranging from ≈60 to ≈120 nm. The 20 mg mL^{-1} solution was spin-coated on the clean substrates at a rate of 600 rpm for 60 seconds in the first step and 2000 rpm for 5 seconds in the second step, producing films ≈110 nm thick. Some films were annealed on a hot plate at temperatures ranging from 80–180°C for 30 minutes to form different polymorphic phases.

For samples prepared on PEDOT:PSS, the PEDOT:PSS solution was filtered through a 0.45 μm polyvinylidene fluoride (PVDF) filter onto clean Si substrates. The solution of PEDOT:PSS was deposited onto the substrate and spun at 4000 rpm for 45 seconds, producing thin films ≈35 nm thick. The samples were annealed on a hot plate at 150°C for 20 minutes. Fullerene derivative films were then cast on the substrates coated with thin PEDOT:PSS films.

Solvent-free C_{60} and PCBM films were made using thermal vapor deposition. C_{60} films were deposited at a pressure of ~10^{-7} Torr and a rate of 0.3 Å s^{-1} onto Si to form thin films with thicknesses of ≈50 nm. PCBM was deposited at a pressure of ~10^{-7} Torr and a rate of 0.3 Å s^{-1} onto cleaned Si substrates for film thicknesses of ≈60 nm. These conditions are known to

produce PCBM films without degradation.[12] We summarize the details on fabrication conditions and sample polymorphs in Table I.

Table I. Summary of fabrication conditions and resulting sample polymorphs.

Sample	Solvent concentration	Spin rate	Annealing[a]	Polymorph[b]
	(mg mL^{-1})	(rpm)	(^{o}C, minute)	
C_{60}	Vapor deposition		-	D
PCBM-SC	30	2000	-	D
PCBM-EVP	Vapor deposition		-	D
PCBNB-1	16	1000	80, 10	D
PCBNB-2	16	1000	160, 30	CP-I
PCBNB-3	16	1000	180, 30	CP-II
PCBNB-4	16	700	80, 10	D
PCBNB-5	16	700	160, 30	CP-I
PCBNB-6	16	700	180, 30	CP-II
PCBNB-7	20	600	-	D
PCBNB-8	20	600	160, 30	CP-I
PCBNB-9	20	600	180, 30	CP-II
PCBNB-10 (PEDOT:PSS)	16	700	160, 30	CP-I

[a] Samples that were not annealed are labeled with dashes.
[b] The abbreviations of D, CP-I, and CP-II stand for highly disordered, crystalline phase I, and crystalline phase II, respectively.

We used spectroscopic ellipsometry (J. A. Woollam VASE) to measure the sample thicknesses, and tapping-mode atomic-force microscopy (AFM, Asylum Research, MFP-3D system) to characterize sample surface morphologies. Figure 2 shows representative AFM images of PCBM and PCBNB thin-films. Crystalline domains on the micrometer scale can be seen clearly in Figs. 2(a) and 2(b), which are images of PCBNB thin films coated on silicon and PEDOT:PSS substrates and both annealed at 160°C. For the other two samples, PCBNB on silicon annealed at 180°C and evaporated PCBM on silicon, there are no observable features that can be associated with such microscale crystalline domains. The domains observed in the evaporated PCBM films have been shown to be disordered by x-ray scattering.[12] PCBNB films

coated on PEDPT:PSS and annealed at 160°C show an interesting morphology with dislocation-mediated growth spirals.[13] The RMS roughness derived from AFM measurements is <9 nm for PCBM and PCBNB annealed at 160°C, and is ≈2 nm for PCBNB annealed at 180°C.

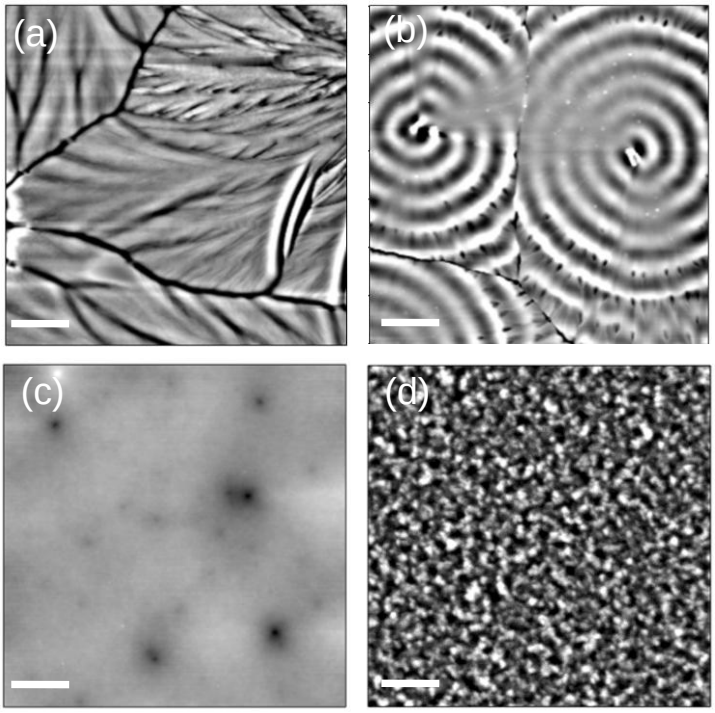

Figure 2. AFM images of representative morphologies: (a) Spin-coated PCBNB film on silicon, annealed at 160°C, (PCBNB-2); (b) Spin-coated PCBNB film on PEDOT:PSS, annealed at 160°C (PCBNB-10); (c) Spin-coated PCBNB film on silicon, annealed at 180°C (PCBNB-3); (d) Evaporated PCBM thin film on silicon (PCBM-EVP). The scale bars are 5 μm for (a), (c), and (d), and 12 μm for (b). The height variation from black-to-white is 30 nm, corresponding to an RMS roughness of less than 9 nm for (a), (b), and (d), and ≈2 nm for (c).

Prior to the TDTR measurement, a thin film of Al with a nominal thickness of ≈80 nm was deposited on the samples via magnetron sputtering. The Al film serves as both a light absorber and a thermoreflectance transducer. A reference sample of 500-nm thick SiO_2 on silicon was loaded inside the sputtering chamber together with the samples during each deposition.

2.2. Time-Domain Thermoreflectance

We used time-domain thermoreflectance (TDTR), a noncontact, pump-probe method, to measure the thermal conductivity and heat capacity of the thin-film samples. In TDTR, a mode-locked Ti:sapphire laser produces a train of pulses (~200 fs in duration) at a repetition rate of 80 MHz. A mechanical delay stage is used to vary the relative optical path length between the pump and probe before they are focused on the sample surface through a single objective lens.[14] The pump beam, modulated by an electro-optical modulator, heats the sample. The probe beam acts as a thermometer by detecting the changes in reflectivity of the Al film produced by changes in temperature. The probe signals are measured by an rf lock-in amplifier. Importantly, the frequency of the pump modulation can be adjusted to vary the sensitivity of the signals to thermal conductivity and the sensitivity to heat capacity.[15] Further details on TDTR can be found in previous publications.[14]

For samples with low thermal conductivity, the temperature rise due to steady-state heating (ΔT_{ss}) may be a concern. However, steady-state heating is not typically a problem for thin-film samples on thermally conductive substrates. In the experiments described below, we used a total laser power of 20 mW and a 5× objective lens that produces a $1/e^2$ spot radius of w_0 = 10.3 μm for both pump and probe. This combination of spot-size and laser power provides excellent signal-to-noise ratio while maintaining an acceptable ΔT_{ss}; ΔT_{ss} < 8 K at room temperature for all samples studied in this work.

3. DATA ANALYSIS AND DISCUSSION

Modeling of TDTR measurements have been discussed in detail previously.[15-17] We analyze the ratio of the in-phase to out-of-phase signal ($-V_{in}/V_{out}$) of the rf lockin that measures

the probe beam to improve the signal-to-noise ratio, increase the sensitivity, and minimize artifacts created by variations of laser spot size and beam overlap as a function of delay time. We use picosecond acoustics to measure the Al transducer thickness.[18,19] Typically, acoustic echoes from the buried sample/substrate interface are also observable and can be used to determine the longitudinal speed of sound of the sample when the sample thickness is known. We use ellipsometry to measure the sample thickness. Picosecond acoustic data for an example PCBNB-on-silicon sample is plotted in Fig. 3.

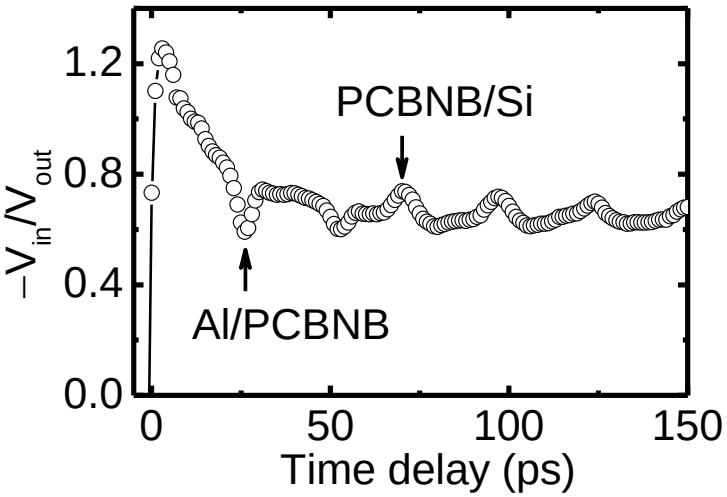

Figure 3. The signal of $-V_{\text{in}} / V_{\text{out}}$ at short time delay. The sample is a multilayer stack of 87-nm Al on a 60-nm PCBNB film spin coated on silicon (PCBNB-1 in Table 1). The labels mark the acoustic echoes for longitudinal acoustic pulses that are generated at the surface, reflect from either the Al/PCBNB or PCBNB/Si interface and return to the surface.

The thermal model contains many parameters: the thickness, volumetric heat capacity, and thermal conductivity of the Al layer ($h_{\text{Al}}, C_{\text{Al}}, \Lambda_{\text{Al}}$), the thin film sample (h, C, Λ), and the substrate (semi-infinite, $C_{\text{sub}}, \Lambda_{\text{sub}}$); thermal conductance of the Al/sample and sample/substrate interfaces (G_1 and G_2); and the beam spot size w_0. For each sample we obtained h_{Al} and the sample film thickness h from picosecond acoustics and ellipsometry, respectively. The thermal

conductivity of aluminum, Λ_{Al} , was calculated using the Wiedemann-Franz law based on the electrical conductivity of the Al layer on the 500-nm SiO_2 reference sample, as measured by a 4-point probe station. C_{Al}, C_{sub}, and Λ_{sub} were taken from literature.[20-22] Due to the ultralow sample thermal conductivities, our measurement is almost completely insensitive to G_1 and G_2. This leaves Λ and C of the sample films as the only adjustable parameters in the thermal model to be obtained by fitting the model prediction to the TDTR data using a software routine that minimizes the deviations between the model and the data.

We quantify the sensitivity of the ratio signal to a parameter in the thermal model in the manner described by Gundrum *et al*.[23] and use the fact that the sensitivities to Λ and C vary with frequency to determine of both parameters. At high modulation frequency (f = 9.8 MHz), the thermal penetration depth in the sample, $\delta = \sqrt{\Lambda / (\pi f C)}$, is $\delta \approx 35$ nm for most of our samples and $\delta \approx 50$ nm for the reference C_{60} sample. A sample with thickness $h >> \delta$ is considered "thermally thick". In this situation, the sensitivity of the ratio signal to Λ and C are similar because heat flow in the sample is mostly governed by the effusivity ($\sqrt{\Lambda C}$). At a sufficiently low modulation frequency, $h << \delta$, the sample is "thermally thin" and the ratio signal becomes more sensitive to Λ and much less sensitive to C because heat flow in the sample is mostly governed by the thermal resistance h/Λ. For intermediate modulation frequencies, the sensitivity to C crosses through zero allowing the sample thermal conductivity to be independently determined.

In Fig. 4, we plot the absolute values of the sensitivity to Λ and C as a function of the modulation frequency for two representative samples consisting of an Al transducer over a PCBNB film on top of a Si substrate. For a thinner PCBNB film with a thickness of 60 nm in

Fig. 4(a), at intermediate modulation frequencies $2<f<5$ MHz, the sensitivity to C is small and Λ can be determined from the data mostly free of error propagation from the uncertainty in C. The optimal modulation frequency, for thicker a thicker PCBNB film of ~120 nm in Fig. 4(b), is reduced to $1<f<2$ MHz for separating Λ and C. At 2 MHz, the ratio of the sensitivities to Λ and C is ≈2 for the 120-nm film and improves to ≈10 for the 60-nm film.

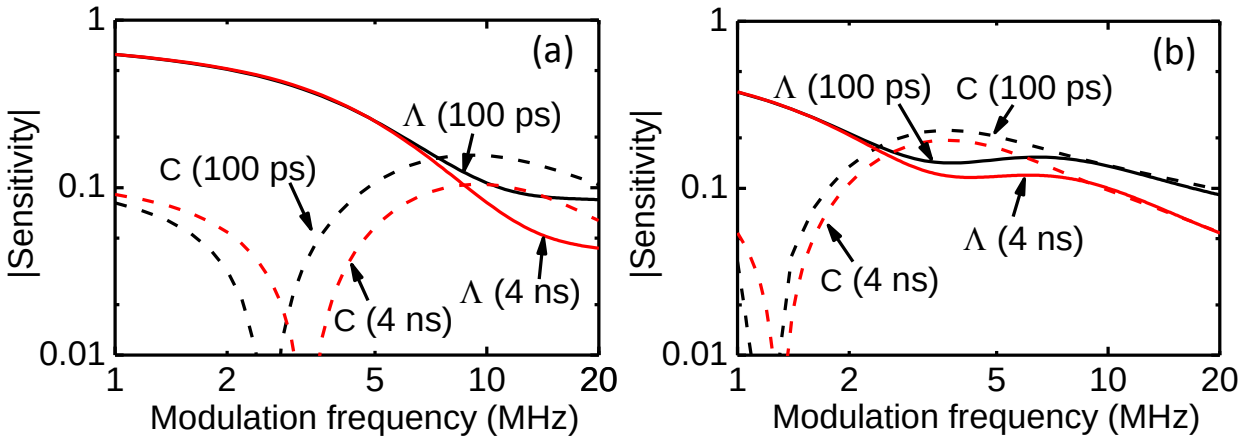

Figure 4. Sensitivity plots of thermal conductivity (solid lines) and heat capacity (dashed lines) of a PCBNB-AS film on silicon as functions of modulation frequency. The thickness of the PCBNB film is 60 nm in (a) and 120 nm in (b). The Al transducer layer is 87 nm. The time delay is set to 100 ps (black lines) or 4 ns (red lines).

The accuracy of Λ measured by TDTR at low frequencies (~1 MHz or less) is subject to pronounced uncertainty in setting the phase.[24] For best performance of TDTR measurements, we measured thinner samples (50–70 nm) at three modulation frequencies, 2.01, 3.55, and 9.8 MHz. The first two frequencies are close to the optimal f (Fig. 4(a)) allowing Λ to be uniquely determined, and the 9.8 MHz data provide additional information to extract C. For each sample, we fitted the data of three modulation frequencies simultaneously to extract Λ and C. Then we used the same value of C for thicker samples with the same chemical structures and polymeric phases; i.e., we assumed that the density of thermally excited vibrational modes is similar for samples of the same type. Thus, in total, we performed frequency-dependent measurements for 5

types of thin samples to obtain both Λ and *C*, including C_{60} (54 nm, highly disordered), PEBM-EVP (57 nm, highly disordered), PCBNB-1 (60 nm, highly disordered), PCBNB-2 (68 nm, crystalline phase I), and PCBNB-3 (70 nm, crystalline phase II). For thicker samples, we conducted measurements at 9.8 MHz only and derived their thermal conductivities using the experimentally determined heat capacities of thinner samples belonging to the same type.

We treat Λ and *C* as adjustable parameters in an analytical heat diffusion model[16] to fit the TDTR data at time delays between 100 ps and 4 ns. The best fit is determined by minimizing the sum of the standard deviation between the model prediction and the measurement data at all three frequencies.

$$\sigma=\sum_{j=1}^{3}\frac{\sum_{i=1}^{n}\left(\frac{R_{\mathrm{m},i}-R_{\mathrm{d},i}}{R_{\mathrm{d},i}}\right)^2}{n}, \qquad (1)$$

where R_m and R_d are the ratios from the model calculation and TDTR data, respectively, at each time delay; *n* is the total number of time delays at each modulation frequency; *j* is an index that denotes each of the three modulation frequencies.

A typical value of σ for the best fit, i.e., the minimum of Eq. 1, is $\sigma_{min}=6\times10^{-4}$. Figure 5 shows examples of contours of constant $\sigma=2\sigma_{min}$ in the two-dimensional parameter space of Λ and *C*. The uncertainties of Λ and *C* as shown in the contour plot in Fig. 5 are ±5% and ±18%, respectively. These uncertainties derive from noise and other imperfections in the data. To evaluate the total uncertainty, we add these uncertainties in quadrature with the uncertainties in Λ or *C* that propagate from uncertainties in the film thicknesses, laser spot size, and the thermal properties of the Al film and substrate. For all five thin samples measured at three frequencies, we use similar approach for uncertainty analysis. For thicker samples that were measured at 9.8

MHz only, we obtain the overall uncertainty of Λ by taking into account the uncertainties and sensitivities for individual parameters in the thermal model.[25]

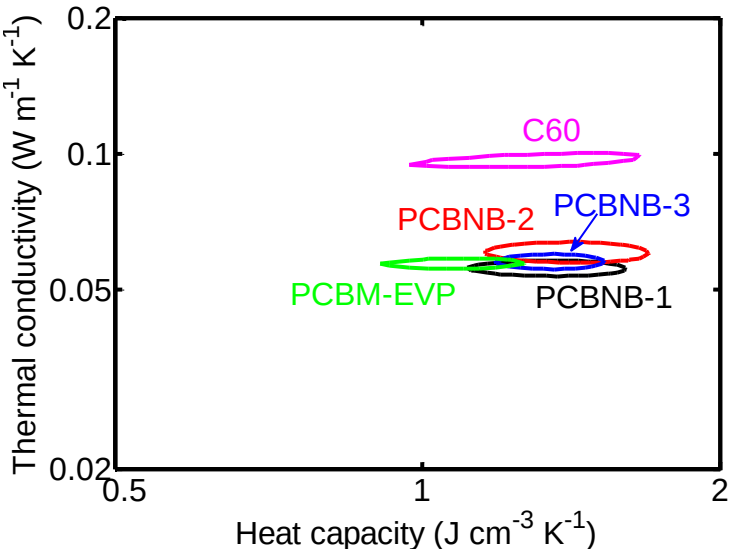

Figure 5. Contour of deviation sum as functions of Λ and *C* for five thin samples. The constant line indicates the combinations of Λ and *C* with a deviation summation that is twice σ_{min}, corresponding to a 95% confidence interval.

We plot the thermal conductivities measured at room temperature in Fig. 6 and summarize these data together with other measurement results in Table II. The thermal conductivities of fullerene derivatives are nearly a factor of 2 higher than those reported by Duda *et al.*.[5] The heat capacities of PCBM and PCBNB derived from frequency-dependent TDTR measurements are in general 1.3–1.4 J cm^{-3} K^{-1}, which falls in the intermediate range between the heat capacities of fullerenes (~1.2 J cm^{-3} K^{-1})[26-29] and simple polymers consisting of aliphatic compounds (~1.8 J cm^{-3} K^{-1}).[30] The heat capacity of the C_{60}/C_{70} compact near room temperature reported in Ref. [10] using the high frequency limit of the 3 omega method is ~20% higher than other literature values.[26-29] The longitudinal speed of sound derived from picosecond acoustics is ≈3.8 nm ps^{-1} for C_{60}, ~40% higher than those of PCBM and PCBNB, indicating that

the fullerene buckyball is stiffer than its derivatives with alkyl sidechains. The longitudinal speed of sound for $PC_{70}BM$ obtained from transient absorption spectroscopy in Ref. [31] is ≈5 nm ps^{-1}, ~80% higher than the values for PCBM and PCBNB reported in this work.

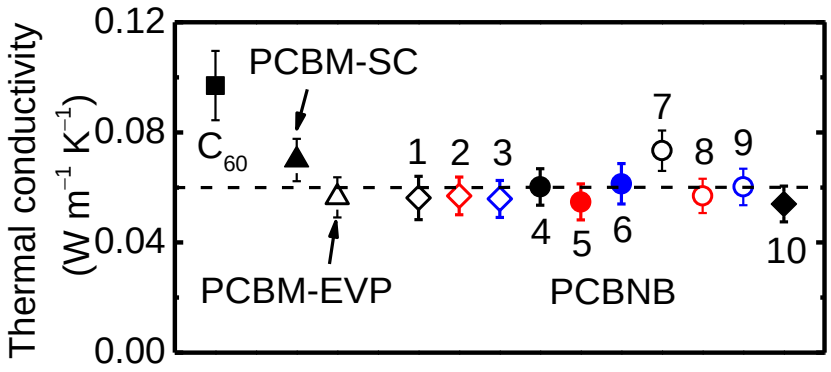

Figure 6. Thermal conductivities of PCBM and PCBNB samples measured at room temperature. The open diamonds, solid dots, and open circles are PCBNB-on-Si samples spin coated from the 16 mg mL^{-1} solvent at a rate of 1000 rpm, the 16 mg mL^{-1} solvent at a rate of 700 rpm, and the 20 mg mL^{-1} solvent at a rate of 600 rpm, respectively. Also shown in Fig. 6 are two highly disordered PCBM samples, one PCBNB-on-PEDOT:PSS sample, and one C_{60} sample used as a reference. The dashed line in Fig. 6 denotes a constant thermal conductivity of 0.06 m^{-1} K^{-1}.

We do not observe a dependence of thermal conductivity of PCBM and PCBNB on fabrication conditions (spin-coating vs. vapor deposition, solvent concentration, spin-coating rate, or heat treatment), sample thicknesses, substrate types (silicon vs. PEDOT:PSS), or sample polymorphs (disordered, crystal phase I, or phase II). Two samples, PCBM-SC and PCBNB-7, have ~20% higher thermal conductivities than the average of the other samples. The origin of this phenomenon is not yet clear, but we speculate that the higher conductivity is due to residual organic solvent used in spin-coating for samples that were not annealed. Residual solvent from chlorobenzene may tend to increase the apparent heat capacity of the sample, leading to a higher thermal conductivity if the effusivity measured at "thermally thick" regime is scaled by the lower heat capacity of a thin sample with thermal treatment.

Table II. Summary of sample parameters and measurement results

Sample	H	Λ	C[a]	v_L
	(nm)	(mW m^{-1} K^{-1})	$\times 10^6$ (J m^{-3} K^{-1})	(nm ps^{-1})
C_{60} (solid square)	54	97±10	1.3±0.3	3.8±0.4
PCBM-SC (solid triangle)	92	70±7	-	2.8±0.3
PCBM-EVP (open triangle)	57	57±7	1.1±0.2	2.9±0.3
PCBNB-1 (black open diamond)	60	56±7	1.4±0.2	2.7±0.3
PCBNB-2 (red open diamond)	68	57±7	1.4±0.3	2.8±0.3
PCBNB-3 (blue open diamond)	70	56±7	1.4±0.2	2.7±0.3
PCBNB-4 (black open circle)	118	73±7	-	2.8±0.3
PCBNB-5 (red open circle)	121	57±6	-	2.8±0.3
PCBNB-6 (blue open circle)	113	60±7	-	2.8±0.3
PCBNB-7 (black solid dot)	125	60±7	-	3.0±0.3
PCBNB-8 (red solid dot)	112	56±7	-	2.8±0.3
PCBNB-9 (blue solid dot)	115	61±7	-	2.8±0.3
PCBNB-10 (solid diamond)[b]	N/A	54±6	-	N/A

[a] We only listed the heat capacities of thinner samples directly derived from TDTR. We label the heat capacities for thicker samples with dashes but used the same heat capacities of thinner samples belonging to the same type for determination of individual thermal conductivities.

[b] The thickness and longitudinal speed of sound for PCBNB-10 (CP-I) are not available due to the existence of the adhesion PEDOT:PSS layer in between the PCBNB film and Si substrate.

To gain insight on the ultralow thermal conductivity of fullerene derivatives, we calculate the theoretical minimum thermal conductivity, Λ_{min}, of PCBNB and PCBM [1]. The minimum thermal conductivity model has successfully predicted the thermal conductivities of amorphous solids and highly disordered crystals. In this model, thermal transport is described by a random walk of vibrational energy on the time and length scales of atomic vibrations and interatomic spacing.

$$\Lambda_{min} = \left(\frac{\pi}{6}\right)^{1/3} k_B n^{2/3} \sum_{i=1}^{3} v_i \left(\frac{T}{\Theta_i}\right)^2 \int_0^{\Theta_i/T} \frac{x^3 e^x}{\left(e^x - 1\right)^2} dx \ , \qquad (2)$$

where k_B is the Boltzmann constant, v_i is the polarization-dependent speed of sound consisting of one longitudinal (v_L) and two transverse (v_T) polarizations, n is the atomic density, and $\Theta_i = v_i\left(\hbar/k_B\right)\left(6\pi^2 n\right)^{1/3}$ is the cutoff frequency with $\hbar$ being the reduced Plank constant. v_L can be directly taken from Table II as measured with picosecond acoustics, and we estimate v_T by scaling v_L with the longitudinal to transverse ratio of C_{60}/C_{70}, $v_L / v_T = 1.74$, as reported in Ref. [10].

In most applications of Eq. (2), the full atomic density n is taken into account in calculating Λ_{min}. Since many of the internal vibrational modes of the fullerene are likely to be localized on the molecule and not contribute significantly to heat transport, we consider a modification of Eq. (2) where we replace n with an effective atomic density n_{eff}. In Fig. 7, we plot Λ_{min} as a function of the effective number of atoms per molecular unit N_{eff} ; $N_{eff} = n_{eff}\Omega$, where Ω = 9.17 Å^3 is the volume per molecular unit of PCBNB derived from the combination of Rutherford Back Scattering (RBS) data for the area density and sample thickness from ellipsometry. The molecular volume of PCBM is only 8% smaller, Ω = 8.47 Å^3. The total number of carbon and oxygen atoms per molecule are 74 for PCBM and 77 for PCBNB. The prediction of the minimum thermal conductivity model agrees with the measurement data (red solid line) at N_{eff} = 2.

N_{eff} =2 is much smaller than what we estimate as the effective number of thermally-excited oscillators. To better illustrate this, we refer to the chemical structure of the C_{60}, PCBM, and PCBNB shown in Fig. 1. Considering that all the carbon atoms of C_{60} are strongly bonded, we follow the approach of Ref. [10] and treat the C_{60} buckyball as an effect single atom with 5 vibrational modes (3 translational and 2 rotational). In the tail structures of PCBM and PCBNB,

each oxygen atom or carbon atom has 2 thermally excited modes. Since the frequencies of the bond-stretching modes and hydrogen-related modes are too high to be excited at room temperature, they should not contribute to the atomic density in the model calculation. This approach leads to a total of 11 and 13 effective atoms in one molecular unit of PCBM and PCBNB, respectively. These values of N_{eff} and corresponding $\Lambda_{\text{min}} \approx 0.2$ W m^{-1} K^{-1} are shown as an open and a filled circle in Fig. 7. By making this assumption, we neglect other surface modes localized on C_{60} individual buckyballs; therefore, this approach probably underestimates the number of thermally excited oscillators and therefore errs on the side of underestimating Λ_{min}.

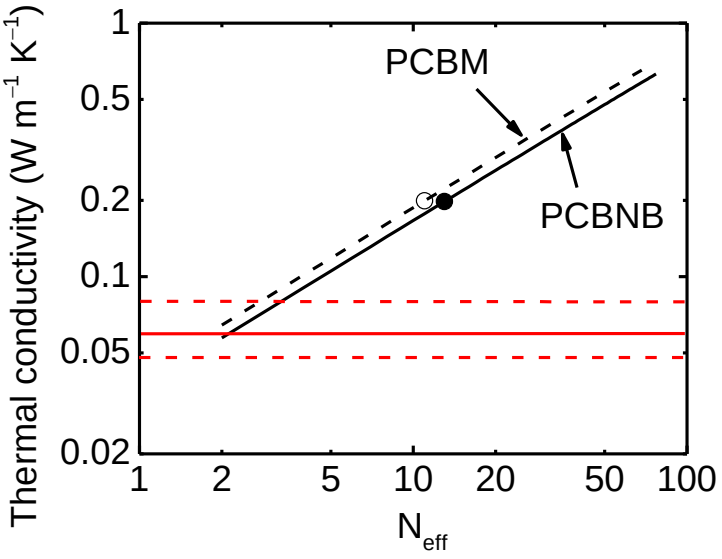

Figure 7. Minimum thermal conductivities as a function of N_{eff}, the effective number of atoms per molecular unit, for PCBM and PCBNB. The open circle and filled circle are model prediction values using N_{eff} =11 for PCBM and N_{eff} =13 for PCBNB, respectively. The measurement data averaged over all 12 fullerene derivative samples (0.06 m^{-1} K^{-1}) is shown as the red solid line with the upper and lower limits (red dashed lines) imposed by the measurement uncertainties.

4. CONCLUSIONS

In summary, we examined the thermal conductivity of [6,6]-phenyl-C_{61}-butyric acid methyl ester (PCBM), and [6,6]-phenyl-C_{61}-butyric acid n-butyl ester (PCBNB) thin films prepared by various deposition conditions. The measured thermal conductivities range from 0.05 $W\ m^{-1}\ K^{-1}$ to 0.06 $W\ m^{-1}\ K^{-1}$ at room temperature for PCBM and spin-coated PCBNB with annealing. The fabrication conditions, substrate types, sample thicknesses and polymorphs do not have significant impacts on the thermal conductivities of PCBM and PCBNB. This class of samples made from fullerene derivatives have ultralow thermal conductivities close to the lowest value of fully dense solids that has been reported.

ACKNOWLEDGEMENT

This work is supported by AFOSR MURI FA9550-12-1-0002. Sample characterization used facilities of the Center of Microanalysis of Materials and the Laser Facility of the Frederick Seitz Materials Research Laboratory (MRL) at UIUC. Portions of the work at UCSB were carried out at the MRL Central Facilities, which supported by the MRSEC Program of the NSF under Award No. DMR-1121053; a member of the NSF-funded Materials Research Facilities Network (www.mrfn.org).

REFERENCES

(1) Cahill, D. G., Watson, S. K., and Pohl, R. O., *Phys. Rev. B* **1992**, 46, 6131-6140.

(2) Chiritescu, C., Cahill, D. G., Nguyen, N., Johnson, D., Bodapati, A., Keblinski, P., and Zschack, P., *Science* **2007**, 315, 351-353.

(3) Keblinski, P. J., Personal communication.

(4) Wei, Z., Chen, Y., and Dames, C., *Appl. Phys. Lett.* **2013**, 102, 011901.

(5) Duda, J. C., Hopkins, P. E., Shen, Y., and Gupta, M. C., *Phys. Rev. Lett.* **2013**, 110, 015902.

(6) Verploegen, E., Mondal, R., Bettinger, C. J., Sok, S., Toney, M. F., and Bao, Z., *Adv. Funct. Mater.* **2010**, 20, 3519-3529.

(7) Zheng, L., Liu, J., Ding, Y., and Han, Y., *J. Phys. Chem. B* **2011**, 115, 8071-8077.

(8) Choi, S.-H., Liman, C. D., Krämer, S., Chabinyc, M. L., and Kramer, E. J., *J. Phys. Chem. B* **2012**, 116, 13568-13574.

(9) Labram, J. G., Kirkpatrick, J., Bradley, D. D. C., and Anthopoulos, T. D., *Phys. Rev. B* **2011**, 84, 075344.

(10) Olson, J. R., Topp, K. A., and Pohl, R. O., *Science* **1993**, 259, 1145-1148.

(11) Rispens, M. T., Meetsma, A., Rittberger, R., Brabec, C. J., Sariciftci, N. S., and Hummelen, J. C., *Chem. Commun.* **2003**, 0, 2116-2118.

(12) Treat, N. D., Mates, T. E., Hawker, C. J., Kramer, E. J., and Chabinyc, M. L., *Macromolecules* **2013**, 46, 1002-1007.

(13) Fujita, J., Kuroshima, S., Satoh, T., Tsai, J. S., Ebbesen, T. W., and Tanigaki, K., *Appl. Phys. Lett.* **1993**, 63, 1008-1010.

(14) Kang, K., Koh, Y. K., Chiritescu, C., Zheng, X., and Cahill, D. G., *Rev. Sci. Instrum.* **2008**, 79, 114901.

(15) Schmidt, A. J., Cheaito, R., and Chiesa, M., *Rev. Sci. Instrum.* **2009**, 80, 094901.

(16) Cahill, D. G., *Rev. Sci. Instrum.* **2004**, 75, 5119-5122.

(17) Schmidt, A. J., Chen, X., and Chen, G., *Rev. Sci. Instrum.* **2008**, 79, 114902.

(18) Eesley, G. L., Clemens, B. M., and Paddock, C. A., *Appl. Phys. Lett.* **1987**, 50, 717-719.

(19) Thomsen, C., Grahn, H. T., Maris, H. J., and Tauc, J., *Phys. Rev. B* **1986**, 34, 4129-4138.

(20) Ditmars, D. A., Plint, C. A., and Shukla, R. C., *Int. J. Thermophys.* **1985**, 6, 499-515.

(21) Desai, P. D., Chu, T. K., James, H. M., and Ho, C. Y., *J. Phys. Chem. Ref. Data* **1984**, 13, 1069-1096.

(22) Fulkerson, W., Moore, J. P., Williams, R. K., Graves, R. S., and McElroy, D. L., *Phys. Rev.* **1968**, 167, 765-782.

(23) Gundrum, B. C., Cahill, D. G., and Averback, R. S., *Phys. Rev. B* **2005**, 72, 245426.

(24) Koh, Y. K., Singer, S. L., Kim, W., Zide, J. M. O., Lu, H., Cahill, D. G., Majumdar, A., and Gossard, A. C., *Journal of Applied Physics* **2009**, 105, 054303-054303-054307.

(25) Cahill, D. G. and Watanabe, F., *Phys. Rev. B* **2004**, 70, 235322.

(26) Allen, K. and Hellman, F., *Phys. Rev. B* **1999**, 60, 11765-11772.

(27) Matsuo, T., Suga, H., David, W. I. F., Ibberson, R. M., Bernier, P., Zahab, A., Fabre, C., Rassat, A., and Dworkin, A., *Solid State Commun.* **1992**, 83, 711-715.

(28) Diky, V. V., Zhura, L. S., Kabo, A. G., Markov, V. Y., and Kabo, G. J., *Fullerene Sci. Techn.* **2001**, 9, 543-551.

(29) Jin, Y., Cheng, J., Varma-Nair, M., Liang, G., Fu, Y., Wunderlich, B., Xiang, X. D., Mostovoy, R., and Zettl, A. K., *J. Phys. Chem.* **1992**, 96, 5151-5156.

(30) Mark, J. E., (Springer, New York, 2006), pp. 145-154.

(31) Kaake, L. G., Welch, G. C., Moses, D., Bazan, G. C., and Heeger, A. J., *J. Phys. Chem. Lett.* **2012**, 3, 1253-1257.